Scientific Research Publishing

Synthesis, Structural Characterization and Computational Studies of Bis(2-Ethylimidazole) Bis(Formato)Zinc(II)-Water (1/1)

**Nana Odette Ngnabeuye[1], Tayo Alain Djampouo[1], Ndosiri Ndoye Bridget[2],
Tanyi Rogers Fomuta[1], Djimassingar Golngar[1,3], Tagne Alain Charly Kuate[1], Ngoune Jean[1*]**

[1]Department of Chemistry, University of Dschang, Dschang, Cameroon
[2]Department of Inorganic Chemistry, University of Yaounde I, Yaounde, Cameroon
[3]Department of Chemistry, Mongo Polytechnique University Institute (IUPM), Mongo, Chad
Email: *jean.ngoune@univ-dschang.org

Abstract

The reaction of 2-ethylimidazole and zinc formate monohydrate in 1:2 ratio in toluene leads to the formation of bis(2-ethylimidazole)bis(formato)zinc(II)-water (1/1), $[Zn(N_2H_8C_5)_2(OCHO)_2] \cdot H_2O$, **1** which has been characterized by several techniques, including elemental and thermal analyses, IR, ^{1}HNMR and ^{13}CNMR spectroscopies, single crystal X-ray diffraction and DFT studies. The results obtained show that this complex crystallizes in the orthorhombic crystal system of the Pbca space group, with cell parameters a = 14.7230(2) Å, b = 7.3880(10) Å, c = 29.0843(4) Å, α = 90°, β = 90°, γ = 90°, V = 3163.73 Å^3 and Z = 8. The zinc center is bound to two molecules of 2-ethylimidazole, two formate molecules in a tetrahedral coordination geometry. One water of crystallization is present in the coordination sphere of the compound. Its molecular crystalline structure is strengthened by O/N-H…O, O-H…π, O-H…H, C-H…O, H…π, π…O and π…π interactions. The optimized structure, frontier molecular orbitals, global reactivity descriptors, molecular electrostatic potential, natural bond orbitals and the Mulliken atomic charges were investigated through theoretical studies.

1. Introduction

Metals have been known to play major roles in many biology and living systems.

Some of these metals being transition elements are used by cells in structurally-constrained binding sites in metalloproteins, where they carry out structural, regulatory or catalytic functions [1]. The biological activities of these metals can be influenced both by speciation and the ligands coordinated to them [2]. For example, zinc which regulates the structure and catalytic action of over 300 enzymes can be found coordinated to different ligand sets such as histidine, glutamate, aspartate, cysteine, etc. The major goal of some bioinorganic chemists is to describe the coordination environment zinc adopts in proteins. Many comprehensive reviews have described the active sites of the metallozinc-enzymes, carboxypeptidase A and carbonic anhydrase [3]. In carboxypeptidase A, zinc is coordinated to two nitrogen atoms from two histidine (His) residues and a glutamate's (Glu) oxygen atom, leaving an open site in the tetrahedral array for the catalytically important water molecule. Meanwhile the active site of carbonic anhydrase comprises of a Zn^{2+} situated at the apex of three histidine residues with an available water molecule for catalysis [3]. Attempts to understand the detailed reaction mechanisms at these zinc-binding centers, alongside the exact nature of the metal coordination environments, are only partially successful in spite of the several spectroscopic and crystallographic investigations executed on these enzymes [4]. The synthesis, study of structures and properties of metal complexes with biologically relevant ligands are currently attracting much attention on account of their promising contribution to understanding the active mechanism of metalloenzymes by means of modeling their metal binding site [5] [6]. Most recently we found profound interest in the reproduction of the active site of carboxypeptidase A through a judicious choice of transition metal that is present in the natural enzyme and a ligand containing nitrogen and/or oxygen donor atoms. In order to expand this family of compounds, we again report the reproduction of the active site of this zinc enzyme by replacing the isopropyl substituent on the imidazole ring in [3] by an ethyl residue. This is realized through the synthesis, characterization and computational studies of bis(2-ethylimidazole)bis(formato)zinc(II)-water (1/1), $[Zn(N_2H_8C_5)_2(OCHO)_2]\cdot H_2O$, **1**.

2. Experimental Section

2.1. Materials and Method

All chemicals used in the isolation and description of this complex were purchased from Aldrich and used without further purification. The synthesis of the complex was carried out in air. Its melting point was uncorrected and measured using an SMP3 Stuart Scientific instrument operating at a ramp rate of 1.5°C/min. Elemental analysis (C, H, N) was performed with a Fisson Instrument 1108 CHNS-O elemental analyzer, while the thermogravimetric analysis was recorded with the aid of a Perkin-Elmer STA 6000 thermo-balance. The IR spectrum was obtained from 4000 - 650 cm^{-1} with a Perkin-Elmer System 100 FT-IR spectrophometer. NMR spectra (400 MHz, ^{1}H and 100 MHz, ^{13}C) were recorded on a

Mercury Plus Variant 400 spectrophotometer operating at room temperature. Proton chemical shift (δ) values are reported in parts per million (ppm) from SiMe$_4$ (calibrating by internal deuterium solvent lock). Peak multiplicities are abbreviated as: singlet, s; doublet, d; triplet, t; quartet, q and multiplet, m. A single crystal of approximately $0.34 \times 0.14 \times 0.10$ mm^3 dimensions was coated with dry perfluoropolyether and glued at the tip of a glass fiber in a cold nitrogen stream [T = 173(2) K] and mounted on top of a goniometer head. The intensity data were collected on a Bruker-Nonius X8 ApexII CCD area detector diffractometer using Mo-K$_a$-radiation source ($\lambda = 0.71073$ Å) fitted with a graphite monochromator. The data collection strategy used was ω and φ rotations with narrow frames (width of 0.50 degree). Instrument and crystal stability were evaluated from the measurement of equivalent reflections at different measuring times and no decay was observed. The data were reduced using SAINT [7] and corrected for Lorentz and polarization effects, and a semi-empirical absorption correction was applied (SADABS) [8]. The structure was solved by direct methods using SIR-2002 [9] and refined against all F^2 data by full-matrix least-squares techniques using SHELXL-2016/6 [10] minimizing $w\,[Fo^2 - Fc^2]^2$. All the non-hydrogen atoms were refined with anisotropic displacement parameters. The hydrogen atoms of the compound were included in the calculated positions and allowed to ride on the attached atoms with isotropic temperature factors (U_{iso} values) fixed at 1.2 times those U_{eq} values of the corresponding attached atoms. Theoretical studies were performed using the Gaussian 09 Revision-A.02-SMP program [11]. The vibrational frequencies, natural bond orbitals, Mulliken atomic charges, electronic structure and geometries of the isolated compound were computed within the density functional theory (DFT) at the hybrid Becke 3-Lee-Yang-Parr (B3LYP) exchange-correlation function with the Lanl2DZ basis set for all the atoms. Molecular orbitals (MO) were visualized using the GaussView 5.0.8 program. Global reactivity descriptors (Ionization energy (I), electron affinity (A), chemical potential (μ), chemical hardness (η), molecular electrophilicity (w), and chemical softness) were computed directly from the energies of the highest occupied molecular orbital (HOMO) and lowest unoccupied molecular orbital (LUMO) using Equations (2)-(6) [12].

$$I = -E_{HOMO} \tag{1}$$

$$A = -E_{LUMO} \tag{2}$$

$$\eta = \frac{I - A}{2} \tag{3}$$

$$S = \frac{1}{2\eta} \tag{4}$$

$$\mu = -\frac{(I + A)}{2} \tag{5}$$

$$\omega = \frac{\mu^2}{2\eta} \tag{6}$$

where, E_{HOMO} and E_{LUMO} are respectively energy values of HOMO (highest occupied molecular orbital) and LUMO (lowest unoccupied molecular orbital). Chemical hardness (η) is associated with the stability of the compound, since it measures the ability of a compound to resist changes in the electron distribution or charge transfer. This implies that high values of chemical hardness indicate more stability and low reactivity of the compound, while molecules with small values of η are said to be chemically soft (*S*) and are highly polarizable and more chemically reactive. Chemical potential (μ) measures the escaping tendency of electrons from a compound in its ground state. High values of chemical potential signify that the molecule is less stable and more reactive [13]. The global electrophilicity index (ω) measures the stabilization in energy of a system, when it acquires an additional electronic charge from the environment [14]. NBO analysis, which figures out the delocalization of electrons during coordination of metal to a ligand was performed using the Gaussian 09 Revision – A.02-SMP program using the Lanl2DZ basis set. For each donor (i) and acceptor (j) atoms, the stabilization energy $E^{(2)}$ associated with the electron delocalization between the donor and acceptor was calculated from the relationship; $E^{(2)} = \Delta Eij = q^{i}F(ij)/(Ej-Ei)$ (where qi = orbital occupancy, Ej, Ei = diagonal elements and F(ij) = off diagonal NBO fock matrix element).

2.2. Synthesis of Bis(2-Ethylimidazole) Bis(Formato) Zinc(II)-Water (1/1), [Zn(N₂H₈C₅)₂(OCHO)₂]·H₂O, 1

The enzyme mimic, $[Zn(N_2H_8C_5)_2(OCHO)_2]\cdot H_2O$, **1** was synthesized by the reaction of 2-ethylimidazole and zinc(II) formate-water (1/2) in toluene as illustrated by Equation (7)

$$Zn(HCOO)_2 \cdot 2H_2O + 2C_5H_8N_2 \xrightarrow{Toluene} \left[Zn(N_2H_8C_5)_2(OCHO)_2 + 2H_2O \right] \quad (7)$$
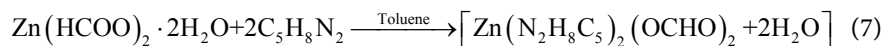
To a colorless toluene (15 mL) solution of zinc(II) formate-water (1/2), $Zn(OHCO)_2\cdot 2H_2O$ (1.00 g, 5.2 mmol) in a 50 mL flask is progressively added 2-ethylimidazole, $C_5H_8N_2$ (1.01 g, 10.4 mmol) in a 1:2 ratio, under magnetic stirring at ambient temperature. The resulting colorless mixture was stirred during 12 hours, leading to formation of a paste-like precipitate, which was filtered and washed trice with acetone and with a DCM: cyclohexane (1:1) mixture. Well formed colorless crystals (1.40 g) of the title compound were then isolated after a partial evaporation of the solvents.

3. Results and Discussion

### 3.1. Physical Properties and Elemental Analysis

The synthesized complex appeared as colorless crystals which melted between 190˚C - 194˚C. A comparison of the percentage of the different elements (C, N, H) analysed (%C: 41.51, %N: 15.90, %H: 5.65) with their theoretical values (%C: 41.75, %N: 16.11, %H: 5.18) confirms the formula, $[Zn(N_2H_8C_5)_2(OCHO)_2]\cdot H_2O$, **1** (MW = 365.69 g/mol) for this complex.

3.2. IR Spectrum of [Zn(N$_2$H$_8$C$_5$)$_2$(OCHO)$_2$]·H$_2$O, 1

The FT-IR spectrum of the compound (Figure 1) displays a slight brought band at 3300 cm^{-1} due O-H vibration of uncoordinated water molecules, while the weak absorption band between 3150 - 3000 cm^{-1} can be attributed to N-H stretching vibration. This observed band, expected around 3300 cm^{-1} is shifted to lower wave number, due to the involvement of these protons in hydrogen bond formation with the oxygen atoms of the formate anion and that of water of crystallization. The weak multiple bands in the interval 2900 - 2800 cm^{-1} are assignable to the valence vibrations of C-H of imidazole or that of the ethyl group. This range is similar to the C-H vibrational frequency observed between 2953 - 2832 cm^{-1} by Fomuta and collaborators when they synthesized the complex salt, [Ag(N$_2$H$_{10}$C$_{11}$)$_2$]PF$_6$ [15]. Moreover, the sharp absorption obtained at 1600 cm^{-1} is due to C=O vibrations while the sharp multiple bands appearing in the interval 1497 and 1473 cm^{-1} correspond to the vibrations of C = C and C = N of the imidazole unit. Furthermore, the broad band between 1396 - 1297 cm^{-1} is due to the vibrations of C-N and N-N of the imidazole ring.

3.3. ^{1}H and ^{13}C Nuclear Magnetic Resonance Spectrum (NMR)

The ^{1}H NMR spectrum shows five families occurring from the weak field to the strong field. In fact, the singlet at δ = 8.5 ppm (1 H, s) is attributable to the N-H imidazolyl proton whereas that observed at δ = 6.8 ppm (1 H, s) is due to the proton of the formate group. The signal noticed at 5.3 ppm (4 H, m) is due to the protons of the CH$_2$ = CH$_2$ group of the imidazole moiety while those observed at 2.6 ppm (2 H, m) arises due to the –CH$_2$- protons of the ethyl substituent on the imidazole ring. The triplet occurring at 1.6 ppm (3 H, t) is assignable to the protons of the –CH$_3$ groups of the ethyl substituent. On the other hand, the ^{13}CNMR spectrum reveals five types of carbon atoms as follows; δ =
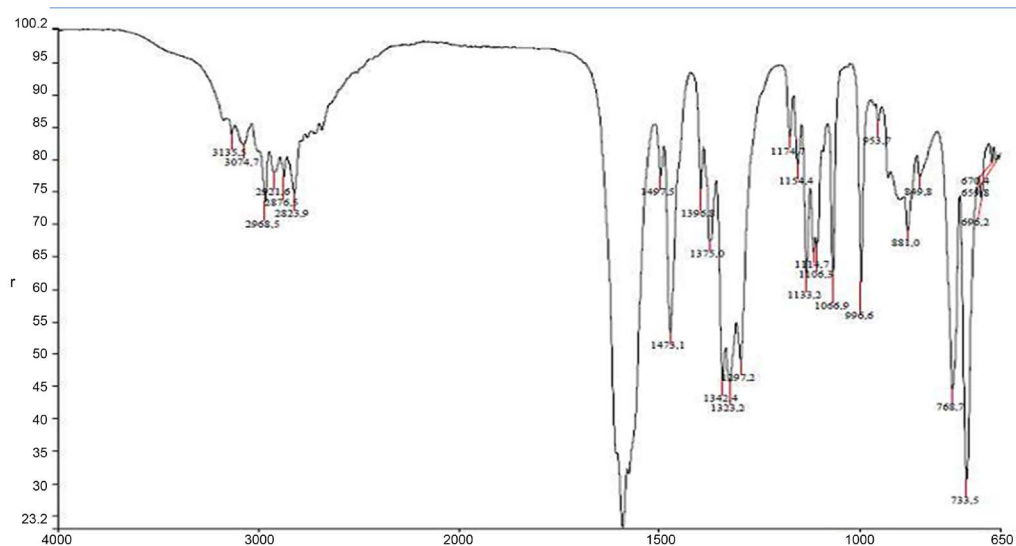

Figure 1. The FT-IR spectrum of [Zn(N$_2$H$_8$C$_5$)$_2$(OCHO)$_2$]·H$_2$O, **1**.

169.54 ppm is assignable to the C = O carbon atom of the formate unit, $\delta = 152.4$ ppm is due to the N = C carbon of the imidazole fractions, $\delta = 121.3$ ppm is attributable to the resonance of the $-CH_2 = CH_2-$ carbons of imidazole, while the signals at $\delta = 21.34$ ppm and $\delta = 12.90$ ppm are due to the carbon atoms of the $-CH_2$ and $-CH_3$ groups of the ethyl substituent respectively.

3.4. Thermogravimetric Analysis

The thermogravimetric curve (**Figure 2(a)**) which measures the effect of heat on the mass of the sample reveals that $[Zn(N_2H_8C_5)_2(OCHO)_2]\cdot H_2O$, **1** is thermally

(a)

(b)
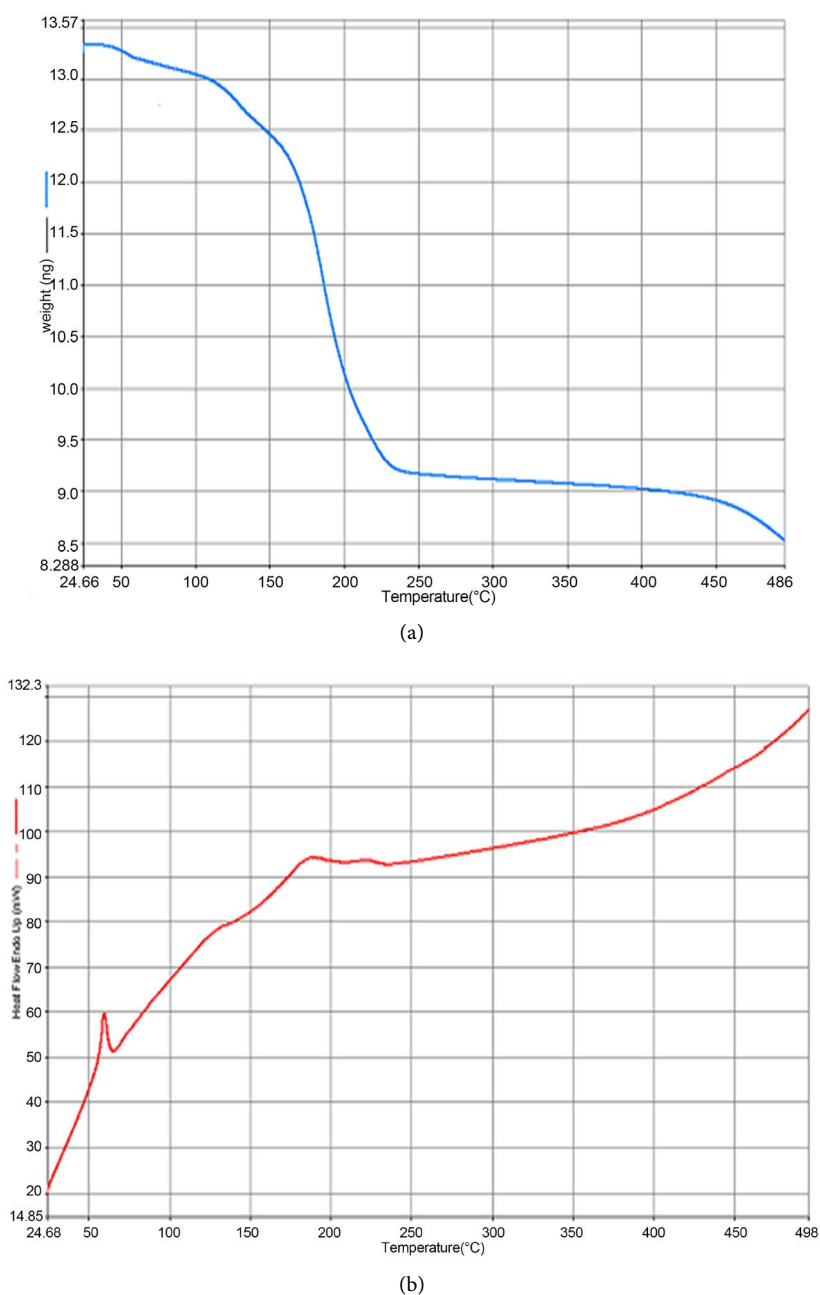
Figure 2. TGA (a) and DTA (b) curves of $[Zn(N_2H_8C_5)_2(OCHO)_2]\cdot H_2O$, **1**.

stable up to 100˚C, after which it undergoes three weight losses. A 2.3% weight loss observed between 50˚C - 90˚C corresponds to the departure of the molecule of water of crystallizaton. The 4.3% weight loss found between 120˚C - 150˚C is attributable to the departure of a formate molecule, while the 18.0% loss in weight between 160˚C and 230˚C is due to the release of a molecule of 2-ethylimidazole. The curve showing the variation in heat content as the material is subjected to heat (Figure 2(b)) indicates an endothermic transformation at 59˚C, corresponding to an enthalpy of 54.7 J·mol^{-1}.

3.5. Crystal Structure Analysis [Zn(N$_2$H$_8$C$_5$)$_2$(OCHO)$_2$]·H$_2$O, 1

Results from X-ray crystal analysis reveals that the synthesized material is a monohydrated neutral compound of formula, [Zn(N$_2$H$_8$C$_5$)$_2$(OCHO)$_2$]·H$_2$O, **1** whose MERCURY and ORTEP views are shown in Figure 3. The crystal data and other structural refinement details of the material are summarized in Table 1 while the selected bond lengths and bond angles are shown in Table 2. The unit cell in which the material crystallizes is shown in Figure 4. The material crystallizes in the Pbca space group of the orthorhombic crystal system and of cell parameters, a = 14.7230(2) Å b = 7.38830(10) Å, c = 29.0843(4) Å, α = 90˚, β = 90˚, γ = 90˚, V =3163.73(7) Å^3 and Z = 8. Moreover, a molecule of the material consist of a Zn(II) metal center, in a pseudo-tetrahedral coordination geometry, constructed by two nitrogen atoms from two monodentate 2-ethylimidazole ligands and two oxygen atoms from two formate anions. The pseudo-tetrehedron is characterized by the bond angles, O(3)-Zn(1)-O(1) = 125.32(5)˚, O(3)-Zn(1)-N(1) = 106.11(5)˚, O(1)-Zn(1)-N(1) = 106.20(5)˚, O(3)-Zn(1)-N(3) = 105.80(5)˚, N(1)-Zn(1)-N(3) = 113.35(5)˚ and distances, Zn(1)-N(1) = 2.0073(13) Å, Zn(1)-N(3) = 2.0195(13) Å, Zn(1)-O(3) = 1.9539(11) Å and Zn(1)-O(1) = 1.9642(12) Å. This mode of coordination of Zn(II) is similar to that found in carboxylpeptidase A. Meanwhile, the bond distances matches well

(a)   (b)
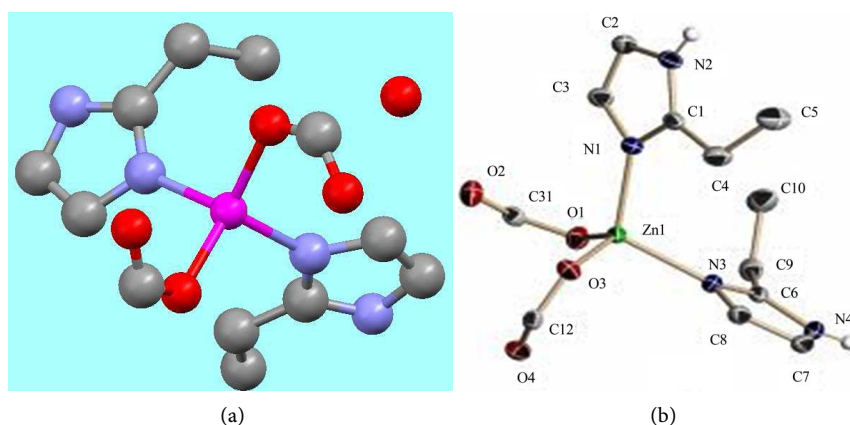
Figure 3. (a) Mercury view (ball and stick) of the crystal structure of [Zn(N$_2$H$_8$C$_5$)$_2$(OCHO)$_2$]·H$_2$O, **1**, Zn (pink), N (blue), O (red); (b) ORTEP view of the structure of [Zn(N$_2$H$_8$C$_5$)$_2$(OCHO)$_2$]·H$_2$O, **1** showing the numbering and labelling of atoms (hydrogen atoms are omitted for clarity).
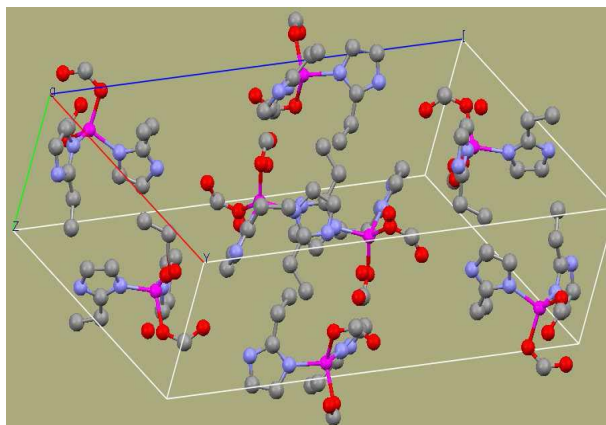
Figure 4. Detailed refinement of the structure of $[Zn(N_2H_8C_5)_2(OOCH)_2]\cdot H_2O$, **1** in its unit cell viewed through the c-axis.

Table 1. Crystallographic data and structure refinement details of $[Zn(N_2H_8C_5)_2(OCHO)_2]\cdot H_2O$, **1**.

Empirical formula	$C_{12}H_{22}N_4O_5Zn$
Molar mass	365.69 g·mol^{-1}
Temperature	173(2) K
Wavelength	0.71073 Å
Crystal system	Orthorhombique
Space group	Pbca
Unit cell dimensions	a = 14.7230(2) Å, b = 7.38830(10) Å, c = 29,0843(4) Å, $\alpha = 90°$, $\beta = 90°$, $\gamma = 90°$
Volume	3163.73(7) Å^3
Z	8
Density (calculated)	1.536 mg/m^3
Absorption coefficient	1.581 mm^{-1}
F(000)	1520
Crystal size	$0.50 \times 0.22 \times 0.18$ mm^3
Theta range for data collection	2.77° to 25.25°
Index ranges	$-17 \leq h \leq 9$, $-8 \leq h \leq 8$, $-34 \leq 1 \leq 13$
Reflection collected	22,220
Independent reflection	2853 [R(int) = 0.0236]
Completeness to theta = 25.25°	99.7%
Absorption correction	Semi-empirical from equivalents
Max and min. transmission	0.7640 and 0.5054
Refinement method	Full-matrix least-squares on F^2
Data/restraints/parameters	2853/4/213
Goodness-of-fit on F^2	1.043
Final R indices [I > 2sigma(I)]	$R_1 = 0.0205$, $wR_2 = 0.0547$
R indices (all data)	$R_1 = 0.0244$, $wR_2 = 0.0562$
Largest diff peak and hole	0.302 and -0.247 e·Å^{-3}

Table 2. Selected bond lengths and angles in $[Zn(N_2H_8C_5)_2(OCHO)_2]\cdot H_2O$, **1**.

Bonds	Values (Å)	Angles	Values (°)
Zn(1)-N(1)	2.0073(13)	O(3)-Zn(1)-O(1)	125.32(5)
Zn(1)-N(3)	2.0195(13)	O(3)-Zn(1)-N(1)	106.11(5)
Zn(1)-O(1)	1.964(12)	O(1)-Zn(1)-N(1)	106.20(5)
Zn(1)-O(3)	1.953(11)	O(3)-Zn(1)-N(3)	100.18(5)
		O(1)-Zn(1)-N(3)	105.80(5)
		N(1)-Zn(1)-N(3)	113.36(5)

Symmetry transformations used to generate equivalent atoms: #1 −x + 1, y, −z + 3/2 #2 −x, y, −z + 1/2.

with those reported in literature [16]. Analysis of the crystal structure of the title compound reveals that the water molecule is uncoordinated but remains isolated in the external coordination sphere of the material. More so, it is found to establish strong intermolecular O/N-H…O (1.917 Å, 1.983 Å, 2.009 Å) interactions, involving its H or O atoms and either the O atom of the formate or an N-H hydrogen atom of the 2-ethylimidazolyl fraction of another $[Zn(N_2H_8C_5)_2(OCHO)_2]\cdot H_2O$, **1** molecule (**Figure 5(a)**). Furthermore, the oxygen atoms of the uncoordinated water are also involved in weak intermolecular O-H…π (2.832 Å), O-H…H (2.394 Å) and C-H…O (2.695 Å) hydrogen interactions (**Figure 5(b)**). Other observed interactions, not involving the water of crystallization, in the material include weak intermolecular N-H…O (2.037Å), C-H…O (2.378 Å, 2.643 Å) (**Figure 6(a)**) established between the hydrogen atoms of 2-ethylimidazole and formate's oxygen atoms, N-H…π (2.886 Å) involving N-H hydrogen and π-electron system of the formate, π…O (3.201 Å) between an oxygen atom and the π-electrons of two formate ions of different molecules and π…π (3.312 Å) occurring between two π-electron systems of different formate ligands (**Figure 6(b)**). It is worth noting that the presence of hydrogen interactions in metalloenzymes helps orientate substrates in appropriate positions to enhance catalytic activity or achieve high catalytic regio- and stereo-selectivities. A remarkable example is the dimanganese complex, $[Mn_2(L)_2(\mu\text{-}O)_2(OH_2)_2](NO_3)_3$ (L is 2, 2':6', 2''-terpyridine) which, when modified by introducing a ligand-based hydrogen bonding group such as –COOH at an appropriate position on L, molecular recognition is achieved, with a regioselectivity > 98% [17]. **Figure 7(a)** shows the ORTEP view of all the hydrogen interactions present in $[Zn(N_2H_8C_5)_2(OOCH)_2]\cdot H_2O$, **1** with values summarized on **Table 3**. All the interactions observed in this material generate a two dimensional crystalline network of varied sized cavities (**Figure 7(b)**) capable of impacted some new properties in this material.

3.6. Theoretical Studies

The theoretical studies of $[Zn(N_2H_8C_5)_2(OOCH)_2]\cdot H_2O$, **1** was performed using the density functional theory (DFT) using the Lanl2DZ basis set at the B3LYP level of theory in the gas phase. The optimized structure of the title compound is
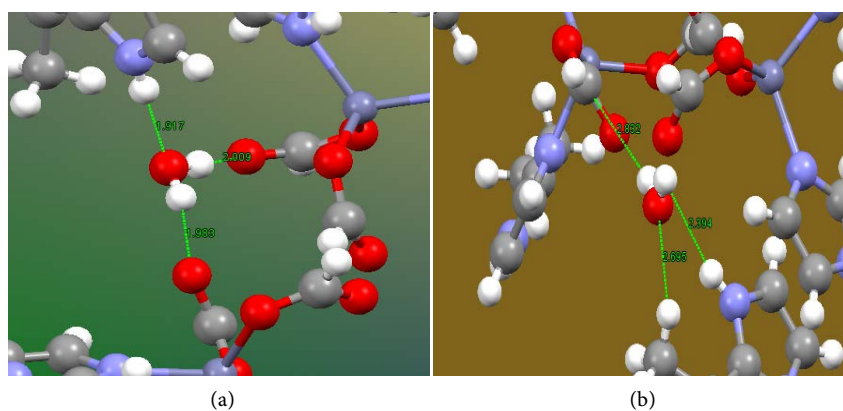
Figure 5. (a) Strong O/N-H…O and (b) Weak O-H…π, O-H…H, C-H…O intermolecular hydrogen interactions involving the oxygen/hydrogen atoms of the uncoordinated water.
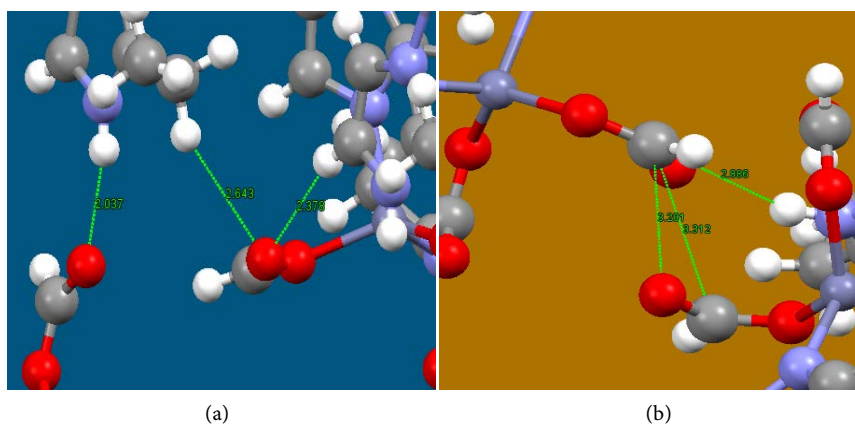
Figure 6. (a)Weak intermolecular N-H…O, C-H…O; (b) N-H…π, π…O and π…π interactions in $[Zn(N_2H_8C_5)_2(OOCH)_2] \cdot H_2O$, **1**.
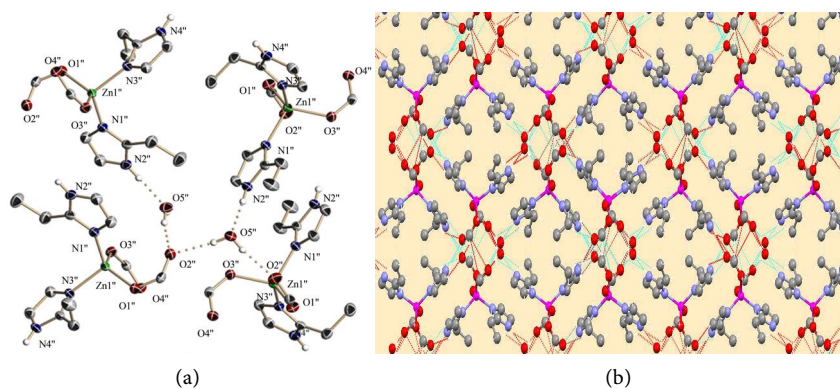
Figure 7. (a) ORTEP view showing hydrogen interactions in $[Zn(N_2H_8C_5)_2(OOCH)_2] \cdot H_2O$, **1**; (b) Two dimensional crystalline network in $[Zn(N_2H_8C_5)_2(OOCH)_2] \cdot H_2O$, **1**.

shown in **Figure 8**. From the figure, it can be deduced that the π-electron system in both the imidazole ring and the formate group are only partially delocalized. However, the experimental geometry is well reproduced in the optimized structure with a comparison presented on **Table 4** and **Table 5**. While all the bond

Table 3. Hydrogen bond distances (Å) and angles (°) for [Zn(N$_2$H$_8$C$_5$)$_2$(OOCH)$_2$]·H$_2$O, **1**.

| D-H...A	d (D-H)	d (H...A)	d (D...A)	<(DHA)
O(5)-H(2O)...O(2)#1	0.827(15)	1.983(15)	2.7989(17)	169(2)
O(5)-H(1O)...O(2)#2	0.819(15)	2.012(16)	2.8033(18)	162(2)
N(4)-H(4N)...O(4)#3	0.832(14)	2.037(15)	2.8562(17)	168.0(18)
N(2)-H(2N)...O(5)#4	0.837(14)	1.918(14)	2.7525(18)	175.3(18)

Symmetry transformations used to generateequivalentatoms #1 −x + 1, −y + 1, −z #2 x + 1, y, z #3 −x + 1, −y + 1, −z + 1 #4 −x + 2, −y + 1, −z + 1 #5 x, y, z − 1.

Table 4. Comparison between experimental and theoretical bond lengths of [Zn(N$_2$H$_8$C$_5$)$_2$(OCHO)$_2$]·H$_2$O, **1**.

[Zn(N$_2$H$_8$C$_5$)$_2$(OCHO)$_2$]·H$_2$O, **1**			
Bond	Experimetal Length (A)	Theoretical Length (A)	Difference between Experimental and Theoretical Lengths (A)
Zn$_8$-N$_9$	2.007	2.091	0.084
Zn$_8$-N$_4$	2.020	2.093	0.073
Zn$_8$-O$_{16}$	1.954	1.969	0.015
Zn$_8$-O$_{19}$	1.964	1.9778	0.014

Table 5. Comparison between experimental and theoretical bond angles of [Zn(N$_2$H$_8$C$_5$)$_2$(OCHO)$_2$]·H$_2$O, **1**.

[Zn(N$_2$H$_8$C$_5$)$_2$(OCHO)$_2$]·H$_2$O, **1**			
Bond angles	Experimental angles (A)	Theoretical Angles (A)	Difference between Experimental and Theoretical angles (A)
O$_{19}$-Zn$_8$-N$_9$	106.20	108.24	2.04
O$_{16}$-Zn$_8$-N$_4$	100.18	111.10	10.92
N$_9$-Zn$_8$-O$_{16}$	106.12	103.94	2.18
N$_4$-Zn$_8$-O$_{19}$	105.80	107.86	2.064
N$_9$-Zn$_8$-N$_4$	113.36	111.52	1.84
O$_{16}$-Zn$_8$-O$_{19}$	125.32	113.54	11.78
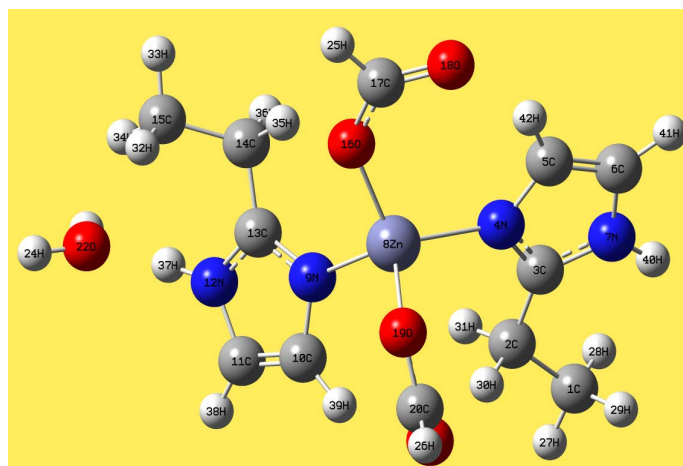
Figure 8. Optimized structure of [Zn(N$_2$H$_8$C$_5$)$_2$(OOCH)$_2$]·H$_2$O, **1** showing its most stable structure and atomic labeling.

lengths around the Zn(II) tetrahedron experienced slight elongation in the optimized structure with a recorded acceptable disparity between 0.014 - 0.084, the O_{19}-Zn_8-N_9, O_{16}-Zn_8-N_4 and N_4-Zn_8-O_{19} angles were enlarged while N_9-Zn_8-O_{16}, N_9-Zn_8-N_4 and O_{16}-Zn_8-O_{19} angles were compressed in the optimized structure. The discrepancy in the O_{16}-Zn_8-O_{19} and O_{16}-Zn_8-N_4 bond angles was exaggerated in the optimized structure. In fact, the experimental O_{16}-Zn_8-O_{19} angle which is 100.18° widens up to 111.10° in the optimized structure, while the experimental O_{16}-Zn_8-N_4 angle of 125.32° is compressed to 113.54° in the optimized structure, giving discrepancies of 10.92° and 11.78° respectively. Some theoretically observed dihedral angles between different atomic planes are shown in Table 6. This difference in the theoretical and experimental geometries could be attributed on one hand to the difference between the experimental model which is in the solid phase and the theoretical model which is in the gas phase. On the other hand, this difference arises from the optimization of the experimental model in a bit to obtain the most stable structure of the material. The frontier molecular orbitals (HOMO and LUMO) (Figure 9) analyses of $[Zn(N_2H_8C_5)_2(OOCH)_2] \cdot H_2O$, **1** and their energy gap reflect the chemical reactivity of the molecule. The HOMO and LUMO energies were obtained from an empirical formula based on the onset of the oxidation and reduction peaks measured by cyclic voltammetry. Recently this energy gap has been used to prove the bioactivity of molecules from intramolecular charge transfer [18]. The HOMO represents the molecular orbital with the ability to donate electrons while the LUMO acts as the electron acceptors.

Table 6. Theoretically observed dihedral angles of $[Zn(N_2H_8C_5)_2(OCHO)_2] \cdot H_2O$, **1**.

	$[Zn(N_2H_8C_5)_2(OCHO)_2] \cdot H_2O$, **1**		
Dihedral angle	Experimental Angles	Theoretical Angles (A)	Difference between Experimental and Theoretical angles (A)
O_{16}-Zn_8-N_4-C_3	158.40	−161.73	3.72971
N_4-Zn_8-N_9-C_{13}	−45.63	−161.73	116.09971
N_4-Zn_8-O_{19}-C_{20}	172.93	119.52	53.40984
N_4-Zn_8-N_9-C_{10}	133.08	84.87	48.20884
N_9-Zn_8-O_{19}-C_{20}	−66.33	56.09	10.23925
O_{16}-Zn_8-O_{19}-C_{20}	57.73	83.01	25.28065

(a)   (b)
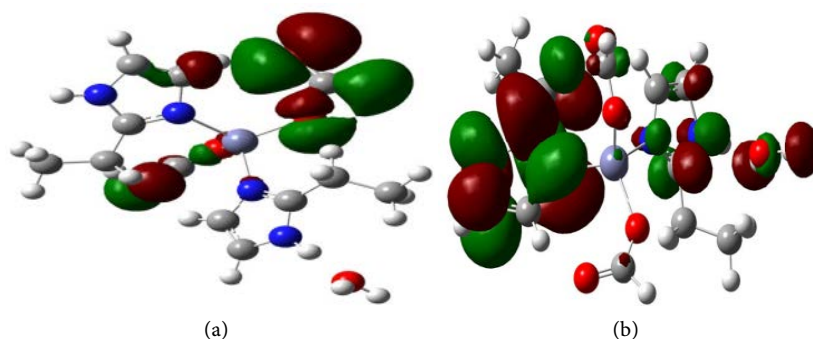
Figure 9. The contour plots of (a) HOMO (−6.093 eV) and (b) LUMO (0.143 eV) orbitals of the studied compound and their energies.

The analysis shows that $[Zn(N_2H_8C_5)_2(OOCH)_2]\cdot H_2O$, **1** has 247 molecular orbitals, 86 occupied molecular orbitals and 161 unoccupied molecular orbitals. The highest occupied molecular orbital, the 86th, has energy of −6.093 eV while the lowest unoccupied molecular orbital, the 87th has energy of 0.143 eV. The red regions of the molecular orbitals (MO) represent the positive phases while the green regions indicate the negative phases. The HOMO-LUMO transition indirectly explains the interactive ability of the target molecule [19]. Moreover, the formate anion makes major contributions to the HOMO with some minor contributions from the carbon atoms of one imidazolyl ring while the major contributions to the LUMO are made by the imidazolyl ring and the water of crystallization, with minor contributions from the formate ion. The molecular electrostatic potential map analysis shows that the oxygen atoms of the formate group constitute the region with the most negative surface potential while the hydrogen atoms of water and that of the N-H imidazole ring possess the most positive electrostatic surface potential. Hence, the oxygen atoms of the formate groups are susceptible to electrophilic attacks while the aforementioned hydrogen atoms are susceptible to attacks by nucleophiles. The global reactive descriptors of this material were calculated using the E_{HOMO} and E_{LUMO}. The results obtained are presented on Table 7. In addition, the theoretical vibrational frequencies and corresponding assignments of the complex were investigated using LanL2DZ basis set and the results obtained are shown on Table 8. The table shows a shift in O-H, N-H and C-H vibrations compared to values obtained experimentally and those reported in literature. However, the theoretical C = O stretching vibrations at 1606 cm^{-1} is similar to that observed experimentally at 1600 cm^{-1} and the values reported in literature. The Natural Bond Orbital (NBO) analysis of $[Zn(N_2H_8C_5)_2(OCHO)_2]\cdot H_2O$, **1** which stresses the role of intermolecular orbital interaction in the material, particularly the charge transfer was carried out by considering all possible interactions between filled donor and empty acceptor NBOs and by estimating their energetic importance by second-order perturbation theory [20]. This analysis which also studies the delocalization of electrons when the hybrid orbitals of the ligands are overlapped with the hybrid orbitals of the metal ions is effective for the study of intra and intermolecular binding. When the stabilization energy, $E^{(2)}$ is high, the interaction between the electron donor

Table 7. Global reactivity descriptors of the complexes.

Descriptor	Value
Ionization energy (I) (eV)	−6.093
Electron affinity (A) (eV)	0.143
Chemical potential (μ) (eV)	2.975
Chemical hardness (η) (eV)	3.118
Energie gap (eV)	6.235
Electrophilicity index (ω) (eV)	1.420

Table 8. Theoretical IR vibrational frequencies (cm⁻¹) of [Zn(N₂H₈C₅)₂(OCHO)₂]·H₂O, **1** and their assignment.

Assignment	Frequency (cm⁻¹)	Assignment	Frequency (cm⁻¹)
$\tilde{\nu}$ (O-H) *wat, as*	3874	$\tilde{\nu}$ (C = C) *im, t*	1589.13
$\tilde{\nu}$ (O-H) *wat, ss*	3708	$\tilde{\nu}$ (C-H) *et, r*	1542.04
$\tilde{\nu}$ (N-H) *im, s*	3692	$\tilde{\nu}$ (C = N) *im, s*	1518.11
$\tilde{\nu}$ (C-H) *im, s*	3328	$\tilde{\nu}$ (C-H) *form, r*	1396.48
$\tilde{\nu}$ (C-H) *et, as*	3146	$\tilde{\nu}$ (C-O) *form, ss*	1298.2
$\tilde{\nu}$ (C-H) *et, ss*	3045	$\tilde{\nu}$ (Zn-O) *as*	414.42
$\tilde{\nu}$ (C-H) *form, s*	3031	$\tilde{\nu}$ (Zn-O) *ss*	385.32
$\tilde{\nu}$ (C = O) *form, ss*	16067		

$\tilde{\nu}$: vibration, *wat*: water, *im*: imidazole, *et*: ethyl, *form*: formate, *s*: stretching, *as*: asymmetric stretching, *ss*: symmetric stretching, *t*: twisting, *r*: rocking.

and acceptor is said to be strong. This also indicates a greater extent of conjugation in the whole system. The stabilization energies, $E^{(2)}$ deduced from the NBO calculations for the most significant intramolecular charge transfer interactions are reported in Table 9 for the coordinating atoms and the Zn(II) metal atom. Meanwhile, Table 10 indicates the stabilization energies, $E^{(2)}$ for the coordinating atoms and other atoms or group of atoms in the molecules. The strongest interaction in [Zn(N₂H₈C₅)₂(OCHO)₂]·H₂O, **1** is that involving the donation of a lone pair of electrons from N4 to the Zn8 anti-bonding orbital with an electron delocalization of 0.287, thereby stabilizing the material by 35.17 kcal/mol. The second strongest interaction is due to the delocalization of the electrons from the lone pair of O19 with LP*(6)Zn8 with occupancy of 0.287, stabilizing the complex by 34.48 kcal/mol, while the third strongest interaction involves the lone pair of N9 with LP*(6)Zn8 with an ED value of 0.287, stabilizing the complex by 30.96 kcal/mol. In addition, the donation of the lone pair of O16 to LP*(7)Zn8 and an ED value of 0.126 stabilized the complex by 30.97 kcal/mol. Again, the NBO results further indicated the absence of metal-ligand charge transfer with all $E^{(2)} \leq 2.5$ kcal/mol, except that of LP*(6)Zn8 to Ry*(1)N4 whose $E^{(2)}$ is 7.61 kcal/mol. The intramolecular hyper conjugative interaction of the π*C3-N4 distributed to the π*C5-C6 has a stabilization energy of 25.16 kcal/mol while the conjugation of π*N9-C13 with C10-C11 of the imidazolyl ring was accompanied by a stabilization energy of 28.75 kcal/mol. Moreover, the intramolecular charge transfer interactions from LP(1)N7 to π*C3-N4, LP(1)N12 to π*N9-C13, LP(3)O16 to π*C17-O18, and LP(3)O19 to π*C₂₀-O₂₁ have $E^{(2)}$ values of 59.80 kcal/mol, 64.98 kcal/mol, 64.40 kcal/mol and 79.76 kcal/mol respectively. These results indicate the presence of electron delocalization from the first lone pair of electrons from N7 atoms to the neighboring C3-N4 and first lone pair of electrons from N12 to neighboring N9-C13 and C10-C11. Furthermore, electron delocalization also occurred from the second lone pair of electrons from O18 to O16-C17 and the third lone pair of electrons

Table 9. The second order perturbation energies E$^{(2)}$ (kcal/mol) of the most important charge transfer interactions (donor-acceptor) of **1**.

Donor (i)	ED (i)	Acceptor (j)	ED (j)	E$^{(2)}$ (Kcal/mol)	Ej-Ei (au)	Fij (au)
LP(1)N4	1.844	LP*(6)Zn8	0.287	35.17	0.57	0.130
LP(1)N9	1.847	LP*(6)Zn8	0.287	30.96	0.57	0.123
LP(2)O16	1.857	LP*(6)Zn8	0.287	28.13	0.70	0.130
LP(2)O16	1.857	LP*(7)Zn8	0.126	30.97	0.72	0.134
LP(2)O19	1.852	LP*(6)Zn8	0.287	34.48	0.68	0.142

(*) indicates anti-bonding, LP (A) is a valence lone pair orbital on atom A, ED is electron delocalization, F (i, j) is the Fock matrix elements (a. u) between i and j NBO.

Table 10. The second order perturbation energies E$^{(2)}$ (kcal/mol) of the most important charge transfer interactions for other atoms/groups within **1**.

Donor (i)	ED (i)	Acceptor (j)	ED (j)	E$^{(2)}$ (Kcal/mol)	Ej-Ei (au)	F(i, j) (au)
LP(1)N7	1.58316	π*C3-N4	0.44158	59.80	0.26	0.112
LP(1)N7	1.58316	π*C5-C6	0.24836	26.32	0.31	0.084
π*C3-N4	0.44158	π*C5-C6	0.24836	25.16	0.05	0.052
LP(1)N12	1.55109	π*N9-C13	0.44853	64.98	0.25	0.113
LP(1)N12	1.55109	π*C10-C11	0.26411	29.64	0.29	0.087
π*N9-C13	0.02694	π*C10-C11	0.26411	28.75	0.04	0.052
LP(3)O16	1.71185	π*C17-O18	0.26430	64.40	0.28	0.121
LP(2)O18	1.88011	π*O16-C17	0.06486	20.87	0.66	0.107
LP(3)O19	1.68120	π*C20-O21	0.03846	79.76	0.25	0.128

(*) indicates anti-bonding, LP (A) is a valence lone pair orbital on atom A, ED is electron delocalization, F (i, j) is the Fock matrix elements (a. u) between i and j NBO.

from both O16 and O19 to C17-O18 and C20-O21 respectively. The Mulliken atomic charges of $[Zn(N_2H_8C_5)_2(OCHO)_2]\cdot H_2O$, **1** were also calculated by NBO analysis using B3LYP method and the results obtained are presented in Table 11. The atoms, C1, C2, N4, N7, N9, C10, C11, N12, C14, C15, O16, O18, O2 and O22 possess negative charges while C3, Zn8, C13, C17, C20 are positively charged. The maximum negative charge is found on water's O22 atom with a value of 0.439. Meanwhile, the maximum positive charge resides on C3 of the imidazolyl ring with a value of 0.318.

4. Conclusion

The novel zinc complex, bis(2-ethylimidazole)bisformatozinc(II)-water (1/1), $[Zn(N_2H_8C_5)_2(OCHO)_2]\cdot H_2O$, **1** has been synthesized and structurally characterized by elemental and thermal analyses, IR, ^{1}HNMR and ^{13}CNMR spectroscopies, single crystal X-ray diffraction and computational studies. The synthesized compound is thermally stable up to 100°C. X-ray results reveal that the zinc metal is in a pseudo-tetrahedral environment and some strong and weak

Table 11. Mulliken atomic charges of some atoms in $[Zn(N_2H_8C_5)_2(OCHO)_2]\cdot H_2O$, **1**.

Atoms	Charge	Atoms	Charge	Atoms	Charge
C1	−0.667	Zn8	1.047	C14	−0.429
C2	−0.405	N9	−0.377	C15	−0.645
C 3	0.329	C10	−0.201	O16	−0.548
N4	−0.375	O22	−0.756	C17	0.062
C5	−0.197	C11	−0.271	O18	−0.361
C6	−0.251	N12	−0.419	O19	−0.499
N7	−0.387	C13	0.318	C20	0.063

intermolecular O/N-H…O, O-H…π, O-H…H and C-H…O hydrogen interactions and other unexpected N-H…π, π…O and π…π interactions insure the crystal packing. Moreover, the coordination environment around the Zn(II) centre reproduces well the active sites of carboxypeptidase A. DFT results revealed the most stable structural arrangement of the title compound with an acceptable disparity between theoretical and experimental bond lengths and angles, even though the disparity between the experimental and the theoretical O_{16}-Zn_8-N_4 and O_{16}-Zn_8-O_{19} angles was exaggerated. The theoretical IR vibrational frequencies and the global reactivity descriptors were computed. The descriptors indicated that $[Zn(N_2H_8C_5)_2(OCHO)_2]\cdot H_2O$, **1** is a soft molecule with a low kinetic stability and a high chemical reactivity. The strongest interaction in this material involved the donation of lone pair of electrons from N4 to Zn8 and there was the absence of metal-ligand back bonding charge transfer.

Acknowledgements

Conflicts of Interest

The authors declare no conflicts of interest regarding the publication of this paper.

References

[1] Delangle, P. and Mintz, E. (2012) Chelation Therapy in Wilson's Disease: From D-Penicillamine to the Design of Selective Bioinspired Intracellular Cu(I) Chelators. *Dalton Transactions*, **41**, 6359-6370. https://doi.org/10.1039/C2DT12188C

[2] Amit, P.S., Nagendra, K.K., Akhislesh, K.V. and Gupta, R. (2011) Synthesis, Structure

Anticancer Activity of Copper(II) Complexes of N-Benzyl-2-(Diethylamino) Aceta-mide and 2-(Diethylamino)-N-Phenylethylacetamide. *Indian Journal of Chemistry*, **50A**, 474-483.

[3] Ngoune, J., Dzesse, C.N.T., Dongmo, G.C. and Tane, P. (2011) Compose Modele des Metalloproteines de Zinc: Synthese et Caracterisation du Complexe Bisformato-bis (2-isopropylimidazole)zinc(II). *Cameroon Journal of Experimental Biology*, **7**, 16-21. http://www.ajol.info/browse-journals.php https://doi.org/10.4314/cajeb.v7i1.69787

[4] Bhattacharyya, S., Kumar, S.B., Dutta, S.K., Tiekink, E.R.T. and Chaudhury, M. (1996) Zinc(II) and Copper(II) Complexes of Pentacoordinating (N4S) Ligands with Flexible Pyrazolyl Arms: Syntheses, Structure, and Redox and Spectroscopic Properties. *Inorganic Chemistry*, **35**, 1967-1973. https://doi.org/10.1021/ic950594k https://pubs.acs.org/doi/pdf/10.1021/ic950594k

[5] Xu, Y., Wang, R.H., Lou, B.Y., Han, L. and Hong, M.C. (2004) Poly [Iron(II)-Di-l-Imidazole-4,5-Di-Carboxylato-j$^3N^3,O^4:O^5$]. *Acta Crystallographica*, **C60**, m296-m298. https://doi.org/10.1107/S0108270104009813

[6] Gomathi, R. and Ramu, A. (2013) Synthesis, Characterization of Novel Cu(II) Complexes of Isatin Derivatives as Potential Cytotoxicity, DNA Binding, Cleavage and Antibacterial Agents. *International Journal of Innovative Research in Science, Engineering and Technology*, **2**, 4852-4865.

[7] APEX2. Bruker AXS Inc., Madison, Wisconsin, USA, 2007.

[8] (2004) Bruker Advanced X-Ray Solutions. SAINT and SADABS Programs. Bruker AXS Inc. Madison, Wisconsin, USA.

[9] Burla, M.C., Camalli, M., Carrozzini, B., Cascarano, G.L., Giacovazzo, C., Polidori, G. and Spagna, R. (2003) SIR2002. *Journal of Applied Crystallography*, **36**, 1103. https://doi.org/10.1107/S0021889803012585

[10] Sheldrick, G.M. (2015) Crystal Structure Refinement with *SHELXL. Acta Crystallographica*, **C71**, 3-8.

[11] Amsterdam Density Functional (ADF) Version 2007.01. http://www.scm.com

[12] Umadevi, P. and Lalitha, P. (2012) Synthesis and Antimicrobial Evaluation of Imino Substituted 1, 3, 4 Oxa and Thiadiazoles. *International Journal of Pharmacy and Pharmaceutical Sciences*, **4**, 523-527.

[13] Mebi, A.C. (2011) DFT Study on Structure, Electronic Properties, and Reactivity of Cis-Isomers of [(NC$_5$H$_4$-S)$_2$Fe(CO)$_2$]. *Journal of Chemical Sciences*, **123**, 727-731. https://doi.org/10.1007/s12039-011-0131-2

[14] Nazmul, I. and Dulal, C.G. (2012) On the Electrophilic Character of Molecules through Its Relation with Electronegativity and Chemical Hardness. *International Journal of MolecularSciences*, **13**, 2160-2175. https://doi.org/10.3390/ijms13022160

[15] Fomuta, T.R., Ngoune, J., Djimassingar, G., Tayo Alain Djampouo, T.A., Matemb, J.M.N.T., Anguile, J.J. and Nenwa, J. (2017) Synthesis, Rietveld Refinement and DFT Studies of Bis (4,5-Dihydro-1H-Benzo[g]Indazole) Silver(I) Hexafluorophos-phate Complex Salt. *Open Journal of Inorganic Chemistry*, **7**, 102-115. https://doi.org/10.4236/ojic.2017.74007

[16] Kleij, A.W., Kuil, M., Lutz, M., Tooke, D.M. Spek, A.L., Kamer, P.C.J., Van Leeuwen, P.W.N.M., Joost, N.H. and Reek, J.N.H. (2006) Supramolecular Zinc(II)Salphen Motifs: Reversible Dimerization and Templated Dimeric Structures. *Inorganica Chimica Acta*, **359** 1807-1814. https://doi:10.1016/j.ica.2005.06.069

[17] Kirby, J.P., Roberts, J.A. and Nocera, D.G. (1997) Significant Effect of Salt Bridges

on Electron Transfer. *Journal of the American Chemical Society*, **119**, 9230-9236.
https://doi.org/10.1021/ja970176

[18] Marouani, H., Raouafi, N., Akriche, T., Al-Deyab, S.S. and Rzaigui, M. (2012) Synthesis, Crystal Structure and Computational Studies of 1-Phenylpiperazin-1,4-Diium Nitrate Monohydrate. *Journal of Chemistry*, **9**, 772-779.
https://doi.org/10.1155/2012/826348

[19] Manikandan, J., Rajarathinan, B., Kannan, M., Mnivel, P., Vasuki, G. and Krishna, R. (2014) Crystallographic and DFT Studies on Pyrrolo [1,2-c] Imidazole Scaffolds. *Journal of Crystallography*, **2014**, 1-8. https://doi.org/10.1155/2014/369061

[20] Gangadharan, R.P. and Krishnan, S.S. (2014) Natural Bond Orbital (NBO) Population Analysis of 1-Azanapthalene-8-ol. *Acta Physica Polonica A*, **125**, 18-22.
https://doi.org/10.12693/APhysPolA.125.18

Supplementary Material

Detailed crystallographic data in CIF format for this paper were deposited with the Cambridge Crystallographic Data Centre (CCDC-1850653). The data can be obtained free of charge at https://www.ccdc.cam.ac.uk/structures/ [or from Cambridge Crystallographic Data Centre (CCDC), 12 Union Road, Cambridge CB2 IEZ, UK; fax: +44 (0) 1223-336033; e-mail: deposit@ccdc.cam.ac.uk].